Brazilian Journal of Geophysics (2021) 39(4): 479–488

ISSN 0102-261X
DOI 10.22564/rbgf.v39i3.2099

CONSTRAINTS FOR MAPPING SUBSURFACE CURRENT SOURCES

Nilton Silva [1] , Suzan Sousa de Vasconcelos [2] , Carlos Alberto Mendonça [3]

ABSTRACT. There is a growing interest in the inversion of self-potential (SP) anomalies, in terms of their current sources, as a way to obtain qualitative and quantitative information about dynamical Earth's subsurface processes. For anomalies interpretation based on geobattery models (as in mineral prospecting and contaminated sites characterization), current polarity indicates terminal anodic-cathodic reactions and current strength gives information on their rate, both important parameters in characterizing the spatial distribution of related redox systems. For investigations in hydrogeophysics, current polarity indicates infiltration/exudation points or interfaces with contrasting physical properties and current strength can be associated to seepage velocity, important parameters to remotely access groundwater hydrology. Actually, promising rewards from SP inversion for current sources deeply rely on the reliability in which polarity and strength for a current distribution can be determined from inverting a data set, considering the uncertainty of the inverse problem and noise level found. In this paper we combine existing regularizing procedures to verify in what conditions a single bipolar, man-made current source can be mapped from a tank experiment data set. As a result, we outline a procedure that can be applied in field conditions to tune data inversion parameters in mapping a subsurface current distribution.

Keywords: spontaneous potential, mineral prospecting, contaminated sites characterization, applied geophysics, data inversion.

RESUMO. Há um interesse crescente na inversão de anomalias de Potencial Espontâneo (SP), em termos de suas fontes de corrente, como forma de obter informações qualitativas e quantitativas sobre processos dinâmicos subsuperficiais da Terra. Para interpretações de anomalias baseadas no modelo de geobateria (como na prospecção mineral e caracterização de áreas contaminadas), a polaridade das correntes indica terminais de reações anódico-catódicas e a intensidade das correntes assinala sua taxa, parâmetros importantes na caracterização de sistemas redox. Para investigações hidrogeofísicas, a polaridade da corrente indica pontos de infiltração/exsudação ou interfaces com propriedades físicas contrastantes e a intensidade da corrente associa-se à velocidade de infiltração, parâmetros importantes para acessar remotamente a hidrologia subterrânea. Inversões bem-sucedidas de SP para fontes de corrente dependem da confiabilidade em que a polaridade e a intensidade da distribuição de correntes podem ser determinadas, considerando a incerteza do problema inverso e o nível de ruído. Neste artigo, combinamos procedimentos de regularização existentes para verificar em que condições uma única fonte de corrente artificial bipolar pode ser mapeada, a partir de um conjunto de dados de experimentos em tanque. Como resultado, delineamos um procedimento aplicável em condições de campo para o mapeamento de uma distribuição de corrente subterrânea.

Palavras-chave: potencial espontâneo, prospecção mineral, áreas contaminadas, geofísica aplicada; inversão de dados.

Corresponding author: Nilton Silva

[1] Tec3GEO Geotecnologias Inovativas Ltda., São Paulo, SP, Brazil – E-mail: nilton@tec3geo.com.br
[2] Universidade Federal da Bahia - UFBA, Instituto de Geociências, Departamento de Geofísica, Salvador, BA, Brazil – E-mail: suzanvasconcelos@gmail.com
[3] Universidade de São Paulo - USP, Instituto de Astronomia, Geofísica e Ciências Atmosféricas (IAG), São Paulo, SP, Brazil – E-mail: carlos.mendonca@iag.usp.br

INTRODUCTION

The self-potential (SP) method is a passive geophysical method (Corwin, 1990) based on measurements of the electrical potential at the ground surface (and/or boreholes), established in response to naturally existing current sources in the subsurface (Sill, 1983). A single data value expresses the spatial difference of the electrical potential measured with a high impedance voltmeter connected to similar non-polarizable electrodes, one of them working as reference (or base station). A subsurface current distribution can be estimated from a set of measurements under formulation of a constrained linear inverse problem (Minsley *et al.*, 2007; Mendonça, 2008). This formulation requires a resistivity model as input, which can be obtained from inverting active, source-controlled resistivity or electromagnetic data.

Most interest on SP investigations comes from the fact that SP fields provide a unique sort of information about dynamical processes active in the subsurface (Snieder *et al.*, 2007; Atekwana and Slater, 2009; Revil *et al.*, 2010). It is understood in the light of near-equilibrium thermodynamics, in which SP fields are featured as a secondary field, coupled to primary fluxes of mass, heat or charged species (electrons and ions), respectively from gradients in pressure, temperature or electrochemical potentials (Onsager, 1931; Marshall and Madden, 1959; Sill, 1983). Since the divergence of coupled fluxes is the same (only by changing the divergence sign), and the inversion of remotely measured SP signals gives the divergence of one of such fields, we have cleared a path to use SP data inversion to map sink and source of causative primary fluxes. This interpretation route promises to useful applications in exploration and environmental geophysics.

A major source of SP signals comes from natural redox systems associated to conductive ore bodies (Sato and Mooney, 1960; Sivenas and Beales, 1982; Bigalke and Grabner, 1997; Goldie, 2002; Castermant *et al.*, 2008; Mendonça, 2008) or organic matter biodegradation in contaminated sites (Naudet *et al.*, 2003; Linde and Revil, 2007; Minsley *et al.*, 2007; Revil *et al.*, 2010). Primary field in redox systems is the oxidation-reduction potential (ORP) of close association with oxygen concentration in soil and rock pores. A consistent electrochemical model is available for mineral bodies (Stoll *et al.*, 1995; Bigalke and Grabner, 1997) in which source terms for the secondary electric field are evaluated from assuming a linearized form for the Butler -Volmer equation (Bockris *et al.*, 2001). For ore bodies, cathodic and anodic reactions are thought as being abiotic (not catalyzed by microbes). In the biodegradation scenario, otherwise, terminal reactions are mediated by microbial forms (bacteria mainly) in metabolic processes they are able to harvest energy from ORP gradients. Besides catalyzing reactions, it has been assumed that microbes can further build electron transfer pathways (Naudet and Revil, 2005; Ntarlagiannis *et al.*, 2007; Revil *et al.*, 2010) by threading biological structures with recently discovered conductive nanowires (Reguera *et al.*, 2005; Gorby *et al.*, 2006). Although keeping most elements of abiotic models, a biogeobattery model assumes that electrons can be canalized by conductive biological structures, either alone or in connection with conductive, disseminated minerals (Naudet and Revil, 2005; Revil *et al.*, 2010). Despite mechanisms in electron transfer, polarity of current in a geobattery model indicates anodic (positive) or cathodic (negative) poles of terminal reactions. A reactive scenario picture can potentially be retrieved simply from mapping current polarity. Current strength, in addition, gives information on reactant consumption/generation in terminal reactions. In mineral exploration it can be useful to discriminate material and environmental conditions affecting electrode kinetics at the ore body surface; and contaminated groundwater can become a biodegradation rate proxy, the most important parameter in accessing natural attenuation processes in which buried organic matter is mineralized (Council *et al.*, 2000).

SP signals are also generated as the groundwater flows through permeable geological media by a kind of electrokinetic phenomena termed streaming potential (Delgado *et al.*, 2007). The association of geophysical signals with groundwater flow parameters has enabled a variety of applications in hydrogeophysics, to cite a few: mapping of infiltration pathways in earth dams (Al-Saigh *et al.*, 1994; Panthulu *et al.*, 2001; Rozycki *et al.*, 2006; Sheffer and Oldenburg, 2007) and dyke embankments (Bolèkve *et al.*, 2009) recognition of regional flow pattern in karst (Vichabian and Morgan, 2002; Revil *et al.*, 2005) and crystalline (Morgan *et al.*, 1989; de Medeiros and de Lima, 1999; Fagerlund and Heinson, 2003) terrains; understanding of complex interactions between meteoric and hydrothermal groundwater in volcanic edifices (Revil *et al.*, 2003; Ishido, 2004; Hase *et al.*, 2005; Aizawa *et al.*, 2009). Basically, streaming potential is a kind of interfacial phenomenon associated to electrical double layers (EDL) built up at mineral surface in rock pores. Beyond a critical distance from the mineral surface, unbalanced charge in the EDL is loose enough to be dragged as the fluid pore is actioned by a pressure field. An streaming current along the flow line is formed and counterbalanced by a conduction (ohmic) current that sustains an electric potential (streaming potential) when a quasi-stationary limit is achieved. Streaming and conduction currents have opposite signs and their strength depends both on velocity seepage (or Darcy velocity) and charge excess in the mobile part of the electrical double layer (Bolèkve *et al.*, 2009). For common Si-Al rock forming minerals and pH levels found in natural systems, the streaming current holds an excess of positive charge. In such conditions, negative poles for the conduction current assign infiltration places injection in pumping tests and positive poles exudation points (withdrawal in pumping tests). Source terms are also expected at interfaces with contrasting EDL properties and hydraulic permeability (Sill, 1983).

Expected rewards from SP inversion for current sources are conditioned by the reliability in which current terms (polarity and strength) can be retrieved from data inversion, considering noise level and intrinsic uncertainty of the inverse problem. In fact, since the number of data values is smaller than the number of parameters, the SP inverse problem is undetermined and its solution is then non unique. Even achieving uniqueness with constraints (e.g., solution with minimum Euclidean norm), noise level in data may lead to unstable solutions. Uniqueness and stability in SP data inversion have been achieved by featuring solutions with desirable properties, more specifically, enforcing constraints on compact solutions with compensated kernel sensitivity with depth (Minsley *et al.*, 2007) and some degree of smoothness (as in general discussed in (Aster *et al.*, 2018). In compact solutions, most of current terms are null, an useful property to embody a conceptual feature that current sources are localized, either as battery poles in redox systems or at interfaces in fluid flow problems. Although with no regularizing power, electro neutrality for inverted current distributions may feature solutions with physical consistency (Mendonça, 2008). For ground water problems, electro neutrality is expected when a contrasting structure is encompassed by the resistivity imaging window. It is not the case of large or regional structures extending well beyond the investigated resistivity cube (or slice in 2D models), since in this framework the whole set of currents does not fit in the investigation window.

In this paper we combine existing regularizing procedures and constraints to verify in what conditions a bipolar current source can be mapped from a set of surface data acquired in a tank experiment. Tank data allow idealized conditions to check reliability of such inversion procedures because minor uncertainty arises from noise data (kept under control by properly experiment design) and imperfections in the background resistivity model. A current source procedure that does not work in such favorable conditions can not be trusted for sure when it is working in real exploration scenarios, where substantially more complex SP sources are mapped. As discussed in the conclusion section, a procedure as developed in this tank experiment can be implemented in field conditions to tune regularizing parameters. In the following we present a common notation for SP forward and inverse formulations; explicitly writing equations to handle the position of the reference station in calculations. Finally we describe our tank experiment procedures and present inversion results from applying different regularizing methods and parameters. Although not inverting real SP sources, we think that learning in mapping a simple, man-made current distribution can be useful to define well suited approaches to handle real SP data sets.

THEORETICAL ASPECTS

SP Forward Problem

The evaluation of theoretical SP anomalies from redox (Stoll *et al.*, 1995; Bigalke and Grabner, 1997; Mendonça, 2008) and electrokinetic (Sill, 1983; Wurmstich and Morgan, 1994; Ishido and Pritchett, 1999) geophysical models are basically made in three steps: i) evaluation of the causative primary flux; ii) evaluation of associated current sources; iii) calculation of the corresponding SP anomaly. SP response (step three) is then a simple resistivity forward problem, in which the electric potential is evaluated from given resistivity and current models. In the finite-difference scheme, the subsurface is represented by pixel-like juxtaposed prims representing a resistivity distribution, and discrete values for the electric potential are evaluated at the mesh nodes. Boundary conditions impose null vertical current density at the ground surface and mixed conditions at bottom and lateral edges of the mesh (Dey and Morrison, 1979a,b). In tank modeling, null flow is imposed across the borders and finite-difference equations for narrow (or 2D) tanks (as used here) are found in Mufti (1976). The electric potential at the network nodes is determined by solving the linear system of equations

$$\mathbf{A}\bar{\mathbf{u}} = \mathbf{q} \tag{1}$$

in which $\mathbf{A}$ is the $n \times n$ finite-difference stiffness matrix, $\bar{\mathbf{u}}$ is the n-dimensional vector with the unknown potentials, and $\mathbf{q}$ is the n-dimensional current source vector. The matrix relationship in equation 1 can be sized down by selecting points in which readings were done. For a set of m reading in nodes $j = 1, \cdots, m$ in data vector, $\mathbf{u_o}$, we have

$$\mathbf{u_o} \equiv \mathbf{Q}\bar{\mathbf{u}}, \tag{2}$$

where $m \times n$ matrix $\mathbf{Q}$ is a sampling matrix with Kronecker deltas, $\delta_{\mathbf{j}}^{\mathbf{T}}$, as rows, T denoting vector transposition. By definition the i-th entry in $\delta_{\mathbf{j}}$ is equal to one and the remainders ones are null. By defining an $m \times n$ matrix $\mathbf{R}_\infty$ such that $\mathbf{R}_\infty \equiv \mathbf{Q}\mathbf{A}^{-\mathbf{1}}$, equation 2 becomes

$$\mathbf{u_o} = \mathbf{R}_\infty \mathbf{q}, \tag{3}$$

in which term ∞ assigns potential values taken with respect to a reference point at the infinity. Since entries in vectors $\mathbf{u_o}$ and $\mathbf{q}$ are respectively expressed in volt and ampere, entries in matrix $\mathbf{R}_\infty$ are expressed in ohm. The matrix $\mathbf{R}_\infty$ can be termed as resistance matrix and the linear system in equation 3 can be regarded as a generalized Ohm's law for a resistor network. Rows in the resistance matrix contain model responses from a unitary pole source at the corresponding station, being then a form of numerical Green's function for background resistivity model.

The reference electrode can be lead into account by considering that a SP value, u_k, at profile k-th station, is such that $u_k = \mathbf{r_k^T q}$, with $\mathbf{r_k^T}$ expressing the k-th row of matrix $\mathbf{R}_\infty$. Similarly, the potential, u_{ref}, for the reference station, is such that $u_{ref} = \mathbf{r_{ref}^T q}$. A set of m potential differences assembled in data vector $\mathbf{u}$ then has entries $u_k - u_{ref}$, $k = 1, \cdots, m$. By defining a matrix $\mathbf{R_{ref}}$ with rows $\mathbf{r_k^T} - \mathbf{r_{ref}^T}$, $k = 1, \cdots, m$, equation 3 (relative to a reference at the infinity) can be replaced by $\mathbf{u} = \mathbf{R_{ref}^T q}$, expressing potential differences with respect to a particular reference station. One can note that this formulation allows incorporating more than one reference station as well as gradient measurements taken with a roving array of electrodes.

Current mapping as an inverse problem

Current mapping aims to determine a distribution of current poles, $\mathbf{q} \equiv [q_1, ..., q_n]^\mathbf{T}$, with discrete values q_i at mesh nodes, from a set of m potential differences $\mathbf{u}$=$[u_1, ..., u_m]^\mathbf{T}$ measured at the ground surface (or in boreholes). Using equation 3 as the starting point (only replacing $\mathbf{R}_{ref}$ by $\mathbf{R}$ for simplicity), its inverse formulation configures a linear problem that has non unique solution because the number of stations (m) is smaller than the number of nodes (n). To achieve a unique and stable solutions, further constraints on the space parameters must be incorporated. Constraints in addition must produce consistent solutions with focused distributions, that do not collapse near the ground surface. As worked here, these objectives are pursuit by combining constraints on maximum compactness (MC) (Last and Kubik, 1983), depth inverse variation (DIV) (Li and Oldenburg, 1998), and electro neutrality (EN) (Mendonça, 2008). MC is useful to produce solutions with most null terms close to a limiting value, b, set a priori. We discuss how to determine a proper value for b in the section discussing the inversion results. A depth compensation is necessary to embrace solutions with deeper level sources, thus avoiding current confinement in a superficial equivalent layer and minimum Euclidean norm (MN) producing smooth solutions (Aster *et al.*, 2018). Combined constraints on MN , MC and DIV, meanwhile honoring data and EN condition, require the minimization of functional

$$\Theta(\mathbf{q}) = (\mathbf{u} - \mathbf{Rq})^T \mathbf{C}_e^{-1} (\mathbf{u} - \mathbf{Rq}) + \mathbf{q}^T (\mu_e \mathbf{W}_e + \mu_c \mathbf{W}_c + \mu_z \mathbf{W}_z) \mathbf{q} \qquad (4)$$

subjected to $\sum \mathbf{q}_i = 0$. In equation 4, $\mathbf{C}_e$ is the data covariance matrix; $\mathbf{W}_e$, $\mathbf{W}_c$, and $\mathbf{W}_z$ are respectively MN , MC and DIV diagonal weighting matrices working as regularizing functionals when making quadratic forms with vector $\mathbf{q}$. Matrix $\mathbf{W}_e$ is made equal to the identity matrix. The i-th diagonal entry in matrix $\mathbf{W}_c$ is equal to $(q_i^2 + \epsilon^2)^{-1}$, ϵ chosen as a small, positive number. The MC quadratic form, when minimized, produces most terms equal to zero and a very few ones not surpassing b. For matrix $\mathbf{W}_z$, the i-th entry is equal to z_i^{-1}, z_i being equal to the depth of the i-th node of the mesh. Scalars μ_e, μ_c and μ_z are weighting parameters that tune the importance attributed to each of the quadratic forms in equation 4. The isolated effect from MN , MC or DIV can be accessed by selectively nulling μ_e, μ_c or μ_z.

Defining matrix $\mathbf{W} \equiv \mu_e \mathbf{W}_e + \mu_z \mathbf{W}_z + \mu_c \mathbf{W}_c$, the solution minimizing $\Theta(\mathbf{q})$ under EN condition, $\hat{\mathbf{q}}_n$, is given (Mendonça, 2008) as

$$\hat{\mathbf{q}}_n = \hat{\mathbf{q}} - \frac{\mathbf{b}^T \hat{\mathbf{q}}}{\mathbf{b}^T (\mathbf{R}^T \mathbf{R})^{-1} \mathbf{b}} (\mathbf{R}^T \mathbf{R})^{-1} \mathbf{b} \qquad (5)$$

in which $\mathbf{b}$ is an m-dimensional vector with all entries equal to one and

$$\hat{\mathbf{q}} = \mathbf{W}^{-1} \mathbf{R}^T (\mathbf{R} \mathbf{W}^{-1} \mathbf{R}^T + \mu_e \mathbf{C}_e)^{-1} \mathbf{u}. \qquad (6)$$

Some words are need about computational implementation of MC under EN condition. Since entries in the weighting matrix $\mathbf{W}_c$ are a function of in parameters $\mathbf{q}$, minimization of functional $\Theta(\mathbf{q})$ requires an iterative algorithm procedure. As proposed by (Last and Kubik, 1983), it can be minimized iteratively by fitting residuals from frozen parameters not-exceeding a previously set threshold. In our implementation, EN was applied to each frozen solution, just before computing residuals and updating solutions in the iterative procedure. This in-loop approach imposes EN to each temporary solution all along with the steps in each MC solution.

EXPERIMENTAL DATA

An experimental apparatus was constructed aiming data repeatability and suitable signal-to-noise ratio in elecktrokinetics experiments to assert SP signals from controlled water pumping, a topic to be addressed in a future work. As illustrated in Figure 1, The tank comprises a $26 \times 10 \times 3cm$ porous ceramic piece encapsulated in a Plexiglas tank ($26 \times 18 \times 3cm$) in width, sealed against walls with silicone. The ceramic piece was produced from standard gel sintering using #320 alumina powder (75% in weight), ceramic binder (20%) and volatile binder (5%). To simulate fault discontinuity (a suitable place for SP sources in data inversion), the upper portion of the piece was cross sectioned producing a gap $1.5\,\mathrm{mm}$ wide and $60\,\mathrm{mm}$ deep at $x = 17.8\,\mathrm{cm}$. The medium was saturated with a NaCl aqueous solution with resistivity of $500\,\Omega\,\mathrm{m}$, with upper and bottom tank compartments kept filled with the same solution. Lateral faucets in the tank (not illustrated in the figure) allowed solution flushing upward until homogenization (same in and out resistivity). After a week in rest, when measurements were done, the solution resistivity in the tank chambers was $335\,\Omega\,\mathrm{m}$.

Electric potential readings were taken with a high impedance $(10\,\mathrm{G}\Omega)$ digital multimeter (Agilent, U1252A) connected to spherical, electroplated Ag-AgCl electrodes, with a formal area of about $19\,\mathrm{mm}^2$. A set of 16 electrodes were spread $15\,\mathrm{mm}$ apart, $8\,\mathrm{mm}$ above the surface of the porous material; the leftmost one

serving as reference. A bipolar current source (positive in A, negative in B) was driven by a variable external current source of about $10\,\mathrm{W}$. The current strength was measured with a supplementary U1252A multimeter operating in the current $\mu\mathrm{A}$ mode. To avoid electrode polarization, a square-wave with 2 s steps of on-off-reverse-off (positive at electrode A when 'on') was used. Time series for input current and potential signals were simultaneously recorded at 10 samples per second. At least five amplitudes for the square wave were applied and for each amplitude at least two wave cycles recorded. Synchronous stairs in current and potential time series were then picked, averaged and subjected to linear regression to estimate the electrical resistance for each AB-MN configuration of electrodes. Resistance measurements were repeated for each of the 15 MN pairs along the profile and the results are presented in Table 1.

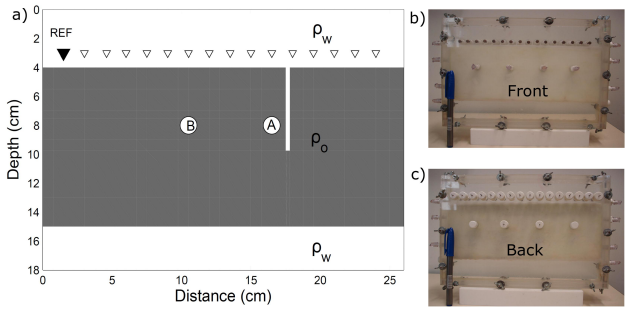

Figure 1. Experimental setup with a porous ceramic piece (gray) of resistivity ρ_0 encapsulated into a Plexiglas tank ($26 \times 18 \times 3cm$); upper and lower chambers filled with aqueous NaCl solution of resistivity ρ_w. Electrodes A (positive) and B (negative) drive electric current, and potential differences are measured by a set of 16 electroplated Ag-AgCl electrodes (triangles); the leftmost one working as reference (REF). Photos of b) front and c) back setup.

Although applying currents from $10\,\mu\mathrm{A}$ to $200\,\mu\mathrm{A}$ in electrodes A and B (and measuring potentials from 10mV to 1000mV in pairs M and N), the resistances thus measured have numerical values equivalent to the electric potential produced by an unitary source $(1\,\mathrm{A})$. Since resistance values are expressed in $\mathrm{k}\Omega$, the equivalent electric potential can be expressed in kV. This correspondence simplifies the data analysis since data inversion results can be compared with unitary values.

Figure 2a shows the objective function for model parameters ρ_w and ρ_0 as the Euclidean norm for a vector with entries $log(v_{c,i}/v_{o,i})$, $i = 1, \cdots, 15$, in which $v_{o,i}$ and $v_{c,i}$ are measured and evaluated potentials. In evaluating $v_{c,i}$ as $v_{c,i}(\rho_w, \rho_0)$, uniform resistivity (ρ_w and ρ_0) is assumed for the tank materials. The best data fitting (Fig. 2b) was found for a pair ρ_w and ρ_0 equal to $346\,\Omega\,\mathrm{m}$ and $994\,\Omega\,\mathrm{m}$. The data fitting from neighboring models in the parameters space (Figs. 2a and 2b) suggests a narrow uncertainty range for the estimated resistivities. Direct measuring in samples from tank chambers gave

Table 1. Transfer resistance evaluated from linear data fitting of voltage readings between electrodes M and N to the electric current applied in electrodes A (positive pole) and B. Thus, the resistance value obtained can be regarded as the potential (in volts) from an input current source of 1 A.

Position (cm)	Resistance (ohm)
3.0	24.7± 0.1
4.5	76.1 ±0.3
6.0	177.1 ±0.2
7.5	345.0 ±1.2
9.0	695.2 ±1.9
10.5	1334.4 ±3.0
12.0	2313.4 ±4.8
13.5	3373.7 ±9.5
15.0	4451 ±25
16.5	5358 ±15
18.0	5945 ±17
19.5	6191 ±20
21.0	6312 ±22
22.5	6360 ±19
24.0	6368 ±20

values of about $335\,\Omega\,\mathrm{m}$, consistent with modeling results. Figure 2c shows the electric potential evaluated in the tank with a finite-difference code (Mufti, 1976) constrained by no current flux tank outward this boundary condition, which makes the equipotentials normal to the tank walls. The resistivity model in Figure 2b (model marked in red) and the finite-difference code evaluating potentials in Figure 2c were used to compute matrix $\mathbf{R}$ in the inversion tests, discussed next.

INVERSION RESULTS

Current mapping can be carried out by considering that source terms may occupy either all nodes of the mesh or may be confined at interfaces. The former approach is valid when a bulk distribution is expected, as current mapping in contaminated sites (Minsley *et al.*, 2007). A distribution at interfaces is expected in groundwater problems (Sill, 1983; Vasconcelos *et al.*, 2014) or redox reactions on conductive ore bodies (Mendonça, 2008; Castermant *et al.*, 2008). To simulate both scenarios, potential values in Table 1a were inverted in three blocks of experiments. In the first block (Fig. 3), a bulk distribution was assumed; in the second and third blocks, (Figs. 4 and 5) only boundary nodes (plus points A and B with true sources) were inverted. In all cases, the objective is identifying the conditions in which a true,

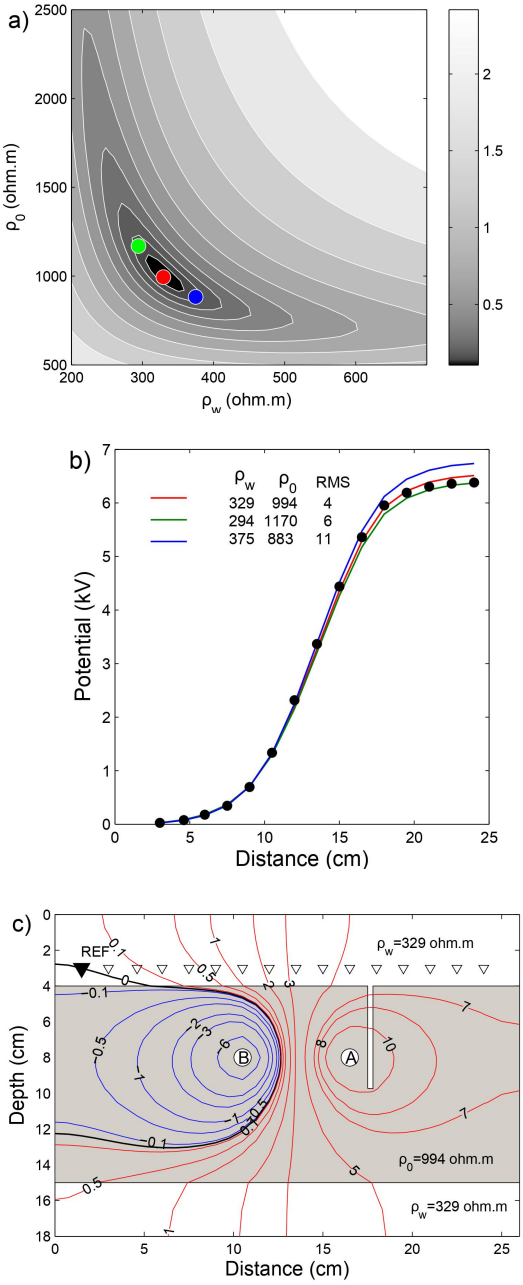

Figure 2. Tank resistivity model and evaluated potentials: a) objective function for model parameters and possible solutions (filled circles in red, green, and blue); b) measured data (black filled circles) and fitting curves (red, green, and blue) from above mentioned resistivity models; c) electric potential in the tank (in kV) evaluated from best fitting data resistivity model (solution marked in red).

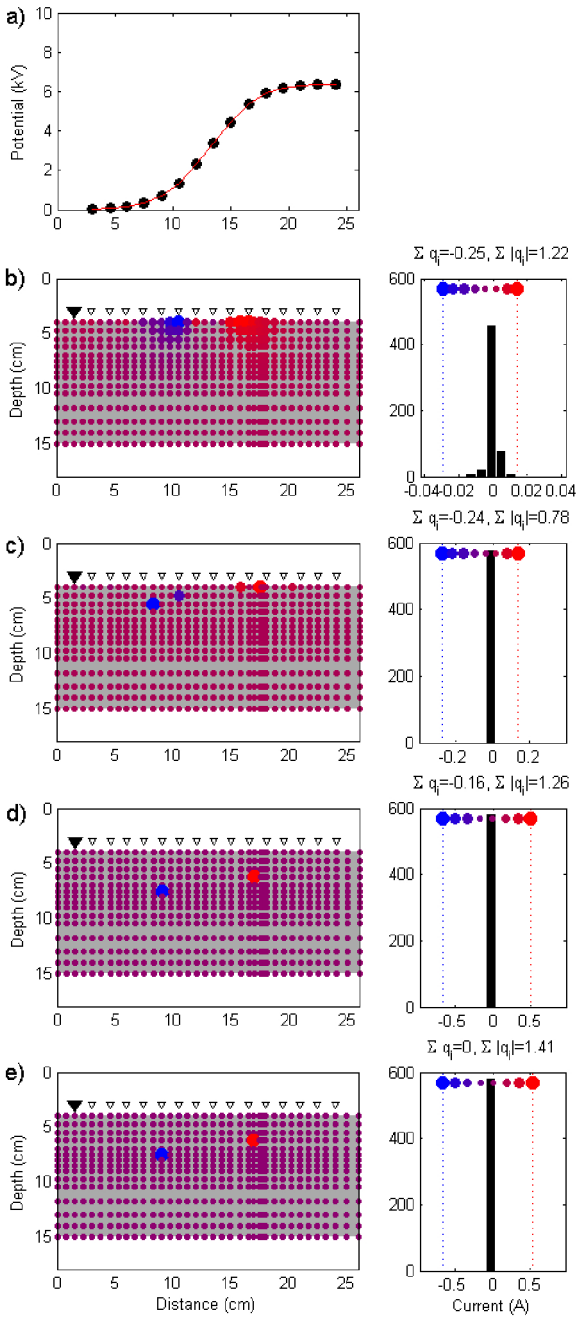

Figure 3. Inversion results for bulk distributions (currents in all mesh nodes): a) data (full circle) and curve fitting (red) from inverted current distributions (below); b) constraint on MN (minimum Euclidean norm) alone; c) constraint on MC (maximum compactness) alone; d) constraint on MC and DIV (depth inverse variation); e) constraint on MC and DIV under EN (electro neutrality) condition.

unitary, and bipolar current source can be mapped.

As shown in Figure 3, the results from bulk mapping were overall ineffective, either in recovering source positions or providing its strength estimates, even when the applied regularizing parameters were $\mu_e = 40$, $\mu_c = 1$, $\mu_z = 20 \times 10^6$. In MN alone, for example, only μ_e is not zero. For MC inversions, the limiting (or freezing) current value was ± 1 A, and convergence was achieved in at most 15 iterations. Because all distributions similarly fit the measured data, only the curve from model e) is shown. Histograms in insets serve as graphical scale for current poles in mapped distributions (left), to access dispersion around the true value (1 A), and present total amount of current Σq_i and $\Sigma|q_i|$.

The solution from only MN constrained (Fig. 3b) is overall meaningless because artificially gives an equivalent layer representation for the sources, a feature not surpassed by MC alone (Fig. 3c). A better source mapping in deeper levels is achieved when combining MC and DIV, in this case with a weighting parameter μ_z as high as 10^6; but solutions featuring downward sources are not straightly paced raising μ_z. No response is noticed when it increases above a threshold and numerical instability arises. The combination of MC, DIV, and EN (Fig. 3d) does not reshape the previous solutions but gives a better estimate $(1.41\,\mathrm{A})$ for the total amount of current in the medium $(2\,\mathrm{A})$. In summary, inversion for a bulk current distribution seems to give only current polarity after well tunning weighting parameters enforcing MC and DIV constraints.

Figure 4 shows results from restricting candidate solutions at a boundary interface (plus points A and B). As for bulk distributions, MN and MC alone (Figs. 4b and 4c) provide equivalent layer solutions, not recognizing the bipolar source in A and B. Weighting constraints on MC and DIV (Fig. 4d) partially accomplished such a task but wrongly estimate the total amount of current $(\sum |qi|)$ as $17.42\,\mathrm{A}$. At least for this test, joining EN to MC and DIV constraints puts the estimated solution very close to the true one (Fig. 4e); error of about 10% in total current. In summary, pole positioning and current parameters (polarity and strength) were substantially improved when working with a node subset at interfaces.

The MC constraint requires a parameter, b, denoting the limiting value imposed for the unknown parameters. In mapping current sources as in SP inversion, this parameter can barely be regarded as known. Results in Figure 5 show that wrong asymmetric distributions (histograms inset) are obtained when b is set too far from the true parameter, in this case out of the range $0.75\,\mathrm{A}$ to $2.0\,\mathrm{A}$. When far below the true value, no smooth solution is achieved because coupled plus-and-minus poles are need to fit data. When far above, the freezing step in the MC algorithm is not effectively actioned and very few current values exceed the threshold b. A solution very close to the true one (Fig. 5d) was obtained when prescribing a slightly greater value (1.5 A) for b. It can be explained by the way the freezing step in the MC algorithm works. When a given parameter exceeds b, it is pushed back to b and kept frozen in iterations. Premature freezing seems to be prevented when setting a slightly greater value for b. In practice, it means that no precise knowledge on maximum current strength is need, but only a slightly majoring value.

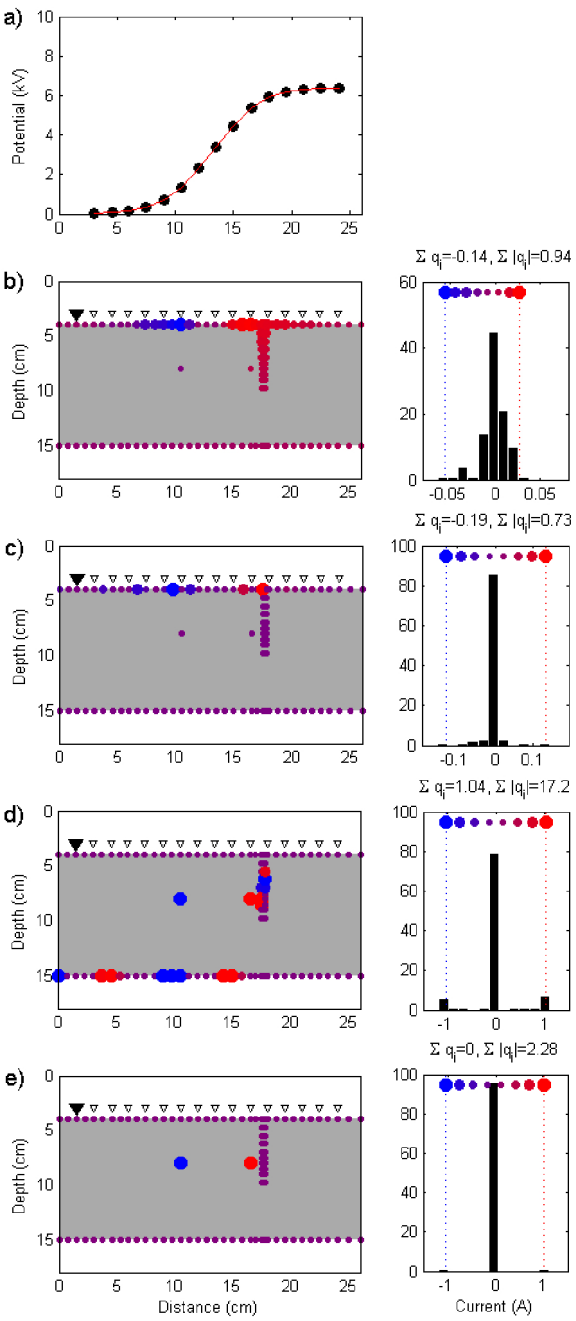

Figure 4. Inversion results for nodes at interfaces and points A and B with the true sources: a) data (full circle) and curve fitting (red) from inverted models; b) MN alone; c) MC alone; d) MC plus DIV; e) MC plus DIV under EN condition. Even when applied, regularizing parameters were equal to $\mu_e = 15$, $\mu_c = 1$, $\mu_z = 760$. For MC inversions, limiting current value was ± 1 A, and convergence was achieved in at most 15 iterations.

CONCLUSIONS

Inversion results from tank experiment suggest that current polarity can fairly be recovered from surface data inversion under tuned constraints on MC (maximum compactness), DIV (depth inversion variation), and EN (electro neutrality). True estimates for source position and current strength are potentially improved when searching current terms in a parameter subspace. In many exploration scenarios a subspace can be configured using the resistivity model already used as input in current source mapping. Based on the resistivity image, a subspace encompassing nodes at interfaces or within bulk conductive targets can be delineated. To

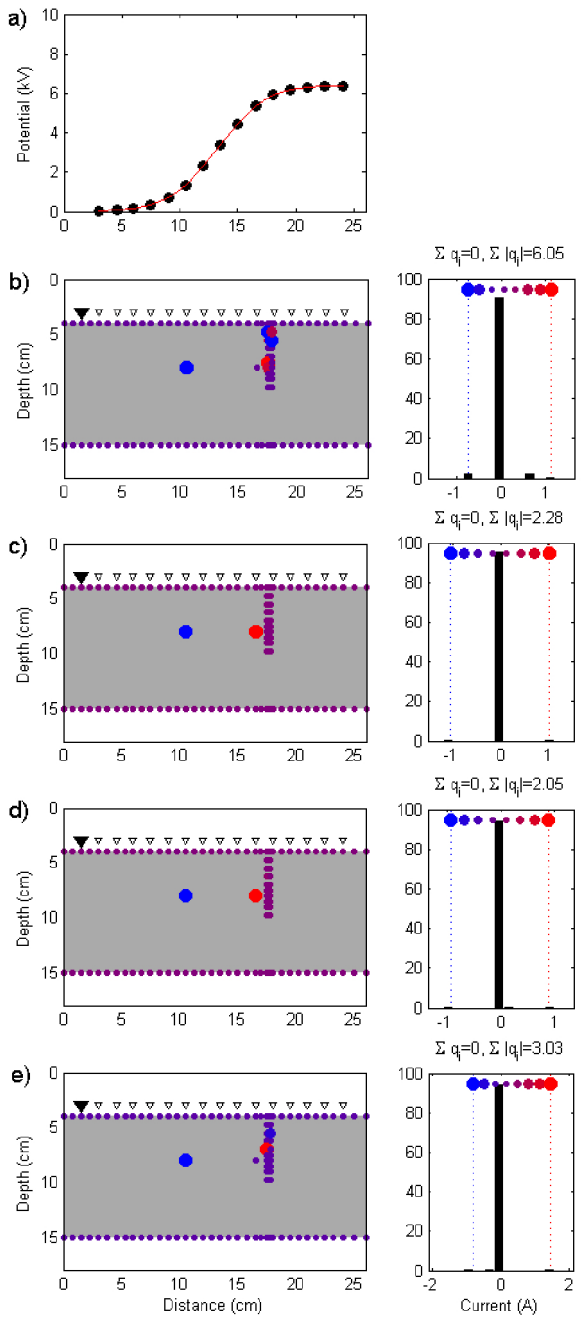

Figure 5. Compact solutions from setting different limiting current values, b, in the MC algorithm: a) data (full circle) and curve fitting (red) from inverted models; b) $b = \pm 0.75$A; c) $b = \pm$ 1.0 A (correct information); d) $b = \pm$ 1.5 A; d) $b = \pm$ 2.0 A. Regularizing parameters were $\mu_e = 15$, $\mu_c = 1$, and $\mu_z = 760$ (same of Fig. 4).

obtain compact solutions, a proper choice for the limiting current value can been done by noticing that no convergence is achieved when this parameter is set too wrong and results are practically invariant when it is set in a narrower range encompassing the true value. Using these criteria, a proper limiting value (or a range for it) can be set from analyzing a set of solutions. However, the main problem in current source mapping (and then in regularized SP inversion) relies on the proper choice of regularizing parameters since they hardly can shape the output solutions. Because the current terms in our experiment were previously known, we could tune parameters until better results were found, of course an unrealizable task when inverting real SP data. However, the equivalence between natural (SP) and artificial current sources allows a procedure to tune weighting parameters, which in many aspects resembles that one tested in tank conditions: i) set a bipolar current source in a borehole (or boreholes); ii) measure the resulting electric field at the ground surface (if possible, at the same SP stations); iii) invert this electric field by tuning the regularizing parameters until better mapping the artificial source; iv) use this weighting set of parameters to invert the SP anomaly. The basic assumption here is that a procedure able to map a known bipolar source can also can be trusted to map an unknown current distribution in similar conditions. In this context, downhole data could be used either to improve the resistivity model (by enlarging the surface data set) or to tune current mapping parameters once the model was obtained. In this condition the proposed procedure can succeed because, if the resistivity model allows data fitting, a solution for the bipolar source does exist, thus making sense tune parameters to find it.

REFERENCES

Aizawa, K.; Ogawa, Y.; Ishido, T. Groundwater flow and hydrothermal systems within volcanic edifices: Delineation by electric self-potential and magnetotellurics. *Journal of Geophysical Research: Solid Earth* **2009**, *114*.

Al-Saigh, N.; Mohammed, Z.; Dahham, M. Detection of water leakage from dams by self-potential method. *Engineering Geology* **1994**, *37*, 115–121.

Aster, R.C.; Borchers, B.; Thurber, C.H. *Parameter estimation and inverse problems*; Elsevier, 2018.

Atekwana, E.A.; Slater, L.D. Biogeophysics: A new frontier in Earth science research. *Reviews of Geophysics* **2009**, *47*.

Bigalke, J.; Grabner, E.W. The geobattery model: a contribution to large scale electrochemistry. *Electrochimica Acta* **1997**, *42*, 3443–3452.

Bockris, J.; Reddy, A.; Gamboa-Aldeco, M. *Modern Electrochemistry: Fundamentals of Electrodics*; Modern electrochemistry / John O'M. Bockris and Amulya K.N. Reddy, Springer US, 2001.

Bolèkve, J.; Revil, A.; Janod, F.; Mattiuzzo, J.; Fry, J.J. Preferential fluid flow pathways in embankment dams imaged by self-potential tomography. *Near Surface Geophysics* **2009**, *7*, 447–462.

Castermant, J.; Mendonça, C.; Revil, A.; Trolard, F.; Bourrié, G.; Linde, N. Redox potential distribution inferred from self-potential measurements associated with the corrosion of a burden metallic body. *Geophysical Prospecting* **2008**, *56*, 269–282.

Corwin, R.F. The self-potential method for environmental and engineering applications. In *Geotechnical an*

Environmental Geophysics: Volume I: Review and Tutorial; Society of Exploration Geophysicists, 1990; pp. 127–146.

Council, N.R.; others. *Natural attenuation for groundwater remediation*; 2000.

de Medeiros, W.; de Lima, O. Origem do potencial elétrico espontâneo em rochas cristalinas fraturadas e sua utilização na locação de poços. *Revista Brasileira de Geofísica* **1999**, *17*, 103–116.

Delgado, Á.V.; González-Caballero, F.; Hunter, R.; Koopal, L.; Lyklema, J. Measurement and interpretation of electrokinetic phenomena. *Journal of colloid and interface science* **2007**, *309*, 194–224.

Dey, A.; Morrison, H.F. Resistivity modeling for arbitrarily shaped three-dimensional structures. *Geophysics* **1979**, *44*, 753–780.

Dey, A.; Morrison, H. Resistivity modelling for arbitrarily shaped two-dimensional structures. *Geophysical prospecting* **1979**, *27*, 106–136.

Fagerlund, F.; Heinson, G. Detecting subsurface groundwater flow in fractured rock using self-potential (SP) methods. *Environmental Geology* **2003**, *43*, 782–794.

Goldie, M. Self-potentials associated with the Yanacocha high-sulfidation gold deposit in Peru. *Geophysics* **2002**, *67*, 684–689.

Gorby, Y.A.; Yanina, S.; McLean, J.S.; Rosso, K.M.; Moyles, D.; Dohnalkova, A.; Beveridge, T.J.; Chang, I.S.; Kim, B.H.; Kim, K.S.; others. Electrically conductive bacterial nanowires produced by Shewanella oneidensis strain MR-1 and other microorganisms. *Proceedings of the National Academy of Sciences* **2006**, *103*, 11358–11363.

Hase, H.; Hashimoto, T.; Sakanaka, S.; Kanda, W.; Tanaka, Y. Hydrothermal system beneath Aso volcano as inferred from self-potential mapping and resistivity structure. *Journal of Volcanology and Geothermal Research* **2005**, *143*, 259–277.

Ishido, T.; Pritchett, J.W. Numerical simulation of electrokinetic potentials associated with subsurface fluid flow. *Journal of Geophysical Research: Solid Earth* **1999**, *104*, 15247–15259.

Ishido, T. Electrokinetic mechanism for the “W”-shaped self-potential profile on volcanoes. *Geophysical Research Letters* **2004**, *31*.

Last, B.; Kubik, K. Compact gravity inversion. *Geophysics* **1983**, *48*, 713–721.

Li, Y.; Oldenburg, D.W. 3-D inversion of gravity data. *Geophysics* **1998**, *63*, 109–119.

Linde, N.; Revil, A. Inverting self-potential data for redox potentials of contaminant plumes. *Geophysical Research Letters* **2007**, *34*.

Marshall, D.J.; Madden, T.R. Induced polarization, a study of its causes. *Geophysics* **1959**, *24*, 790–816.

Mendonça, C.A. Forward and inverse self-potential modeling in mineral exploration. *Geophysics* **2008**, *73*, F33–F43.

Minsley, B.J.; Sogade, J.; Morgan, F.D. Three-dimensional self-potential inversion for subsurface DNAPL contaminant detection at the Savannah River Site, South Carolina. *Water Resources Research* **2007**, *43*.

Morgan, F.; Williams, E.; Madden, T. Streaming potential properties of westerly granite with applications. *Journal of Geophysical Research: Solid Earth* **1989**, *94*, 12449–12461.

Mufti, I.R. Finite-difference resistivity modeling for arbitrarily shaped two-dimensional structures. *Geophysics* **1976**, *41*, 62–78.

Naudet, V.; Revil, A. A sandbox experiment of the relationship between redox and self-potential and its application to the interpretation of self-potential data over contaminant plumes. *Geophysical Research Letters* **2005**, *32*, L11405.

Naudet, V.; Revil, A.; Bottero, J.Y.; Bégassat, P. Relationship between self-potential (SP) signals and redox conditions in contaminated groundwater (DOI 10.1029/2003GL018096). *Geophysical Research Letters* **2003**, *30*, HLS–2.

Ntarlagiannis, D.; Atekwana, E.A.; Hill, E.A.; Gorby, Y. Microbial nanowires: Is the subsurface “hardwired”? *Geophysical Research Letters* **2007**, *34*.

Onsager, L. Reciprocal relations in irreversible processes. I. *Physical review* **1931**, *37*, 405.

Panthulu, T.; Krishnaiah, C.; Shirke, J. Detection of seepage paths in earth dams using self-potential and electrical resistivity methods. *Engineering Geology* **2001**, *59*, 281–295.

Reguera, G.; McCarthy, K.D.; Mehta, T.; Nicoll, J.S.; Tuominen, M.T.; Lovley, D.R. Extracellular electron transfer via microbial nanowires. *Nature* **2005**, *435*, 1098–1101.

Revil, A.; Saracco, G.; Labazuy, P. The volcano-electric effect. *Journal of Geophysical Research: Solid Earth* **2003**, *108*.

Revil, A.; Cary, L.; Fan, Q.; Finizola, A.; Trolard, F. Self-potential signals associated with preferential ground water flow pathways in a buried paleo-channel. *Geophysical Research Letters* **2005**, *32*.

Revil, A.; Mendonça, C.; Atekwana, E.; Kulessa, B.; Hubbard, S.; Bohlen, K. Understanding biogeobatteries: Where geophysics meets microbiology. Technical report, Lawrence Berkeley National Lab.(LBNL), Berkeley, CA (United States), 2010.

Rozycki, A.; Fonticiella, J.R.; Cuadra, A. Detection and evaluation of horizontal fractures in earth dams using the self-potential method. *Engineering Geology* **2006**, *82*, 145–153.

Sato, M.; Mooney, H.M. THE ELECTROCHEMICAL MECHANISM OF SULFIDE SELF-POTENTIALS. *GEOPHYSICS* **1960**, *25*, 226–249. 10.1190/1.1438689.

Sheffer, M.R.; Oldenburg, D.W. Three-dimensional modelling of streaming potential. *Geophysical Journal International* **2007**, *169*, 839–848. 10.1111/j.1365-246x.2007.03397.x.

Sill, W.R. Self-potential modeling from primary flows. *GEOPHYSICS* **1983**, *48*, 76–86.

10.1190/1.1441409.

Sivenas, P.; Beales, F.W. Natural geobatteries associated with sulphide ore deposits, I. Theoretical studies. *Journal of Geochemical Exploration* **1982**, *17*, 123–143.

Snieder, R.; Hubbard, S.; Haney, M.; Bawden, G.; Hatchell, P.; Revil, A.; others. Advanced noninvasive geophysical monitoring techniques. *Annual Review of Earth and Planetary Sciences* **2007**, *35*, 653–683.

Stoll, J.; Bigalke, J.; Grabner, E. Electrochemical modelling of self-potential anomalies. *Surveys in Geophysics* **1995**, *16*, 107–120.

Vasconcelos, S.S.; Mendonça, C.A.; Silva, N. Self-potential signals from pumping tests in laboratory experiments. *Geophysics* **2014**, *79*, EN125–EN133.

Vichabian, Y.; Morgan, F.D. Self potentials in cave detection. *The Leading Edge* **2002**, *21*, 866–871.

Wurmstich, B.; Morgan, F.D. Modeling of streaming potential responses caused by oil well pumping. *Geophysics* **1994**, *59*, 46–56.

N.S.: Construction of experimental setup, quality tests and performance of measurements. Writing about apparatus, tests, and measurements. Figures editing. **S.S.V.:** Inversion program code and writing the inversion methodology, and results. Figures editing. Text formatting according to journal guidelines. Answering reviewers' demands. **C.A.M.:** Conceptualization. Research Guidance. Participation in all stages (experimental and code implementation) - creation, implementation, description, and meeting the demands of reviewers.

Received on April 6, 2021/ Accepted em October 9, 2021.